Mass effects on regrowth rates and activation energies of solid-phase epitaxy induced by ion beams in silicon

A. Kinomura* and J. S. Williams

Department of Electronic Materials Engineering, Research School of Physical Sciences and Engineering, Australian National University, Canberra ACT 0200, Australia

K. Fujii

Osaka National Research Institute, AIST, 1-8-31 Midorigaoka, Ikeda, Osaka 563-8577, Japan

The effect of ion mass on ion-beam-induced epitaxial crystallization of silicon has been examined for five types of ion (C, Si, Ge, Ag, Au) at energies of 1.5, 3.0, and 5.6 MeV. Regrowth rates have been normalized to the number of displacements or nuclear energy deposition at the interface to evaluate the contribution of defect generation to crystal growth. The normalized regrowth rate increased by a factor of 4 with decreasing ion mass from Au to C, showing a similar behavior to dose rate dependences previously reported at lower ion energies. However, the dose rate dependence for 3.0 MeV Au and Ag deviated from this mass dependence curve at low dose rates, indicating that significant cascade density effects (instantaneous dose rate effects) coexist with average dose rate effects. This implies that the crystal growth rate is affected by defect interactions within individual cascades as well as by defect interactions between different cascades. Activation energies measured for four types of ion at 3.0 MeV are also mass dependent and varied from 0.18 to 0.40 eV. These results indicate that ion-beam-induced epitaxial crystallization cannot be characterized by a single activation energy. Our data have been compared with a number of models for ion-beam-induced crystallization and found to be inconsistent with a process controlled by a single defect type. We suggest that several rate-limiting defect processes may be involved and the dominance of a single defect depends on the ion mass (cascade density), average dose rate, and temperature regime. [S0163-1829(99)08323-X]

I. INTRODUCTION

Ion-beam-induced epitaxial crystallization (IBIEC) of silicon has been extensively studied over the past two decades because of possible insight into fundamental crystallization processes and technological importance.[1–4] Ion-beam-induced epitaxy occurs at temperatures as low as 200 °C, while pure thermal solid-phase epitaxy is observed at higher temperatures above 400 °C. Typical activation energies of IBIEC are found to be around 0.3 eV,[3–6] one order of magnitude lower than that of thermal epitaxy (2.7 eV).[7] The dopant dependence and orientation dependence of IBIEC are found to be weaker than those of thermal epitaxy.[3,8,9] A unique feature of IBIEC is that epitaxial crystallization reverts to ion-beam-induced interfacial amorphization (IBIIA) below a zero growth temperature depending on dose rates and ion species.[2,10,11]

The basic mechanism of IBIEC has been discussed in many papers on the assumption that point defects generated by ion irradiation induce crystallization or amorphization. Time-resolved reflectivity was used to measure regrowth rates for comparison with calculated displacement density (vacancy concentration) as a function of depth.[9,12] The regrowth rate was found to closely follow the generated vacancy concentration at the amorphous/crystalline interface. This result suggested that the regrowth rate of IBIEC is associated with point defect generation close to the interface. The contribution of point defects to beam-induced crystallization has been more directly demonstrated in the case of electron-beam-induced epitaxial crystallization.[13] Electron

beam irradiation at energies below the threshold for atomic displacements induced no crystal growth, while irradiation at energies above the threshold induced crystal growth. The origin of ion-beam-induced defects responsible for crystallization was investigated by channeled ion irradiation to reduce defect generation in the crystalline region[6,14] or low-energy ion irradiation to confine most of the nuclear energy deposition in the amorphous region.[15] However, it was difficult to draw definite conclusions as to which region (i.e., the crystalline side, the amorphous region, or exactly at the interface) is the dominant source of the defects for IBIEC.

IBIEC is found to exhibit a weak dose rate dependence of regrowth rates and also for zero growth temperature.[11,16,17] Furthermore, the crystallization induced by pulsed beams showed a dependence of the regrowth rate on pulse frequency.[16] Measured dependences suggested that the lifetime of defects contributing to crystallization was approaching 1 s in some cases and that defect interactions were significant influencing factors. Hence it is impossible to simply correlate the regrowth rate with defect generation or nuclear energy deposition at or near the amorphous/crystalline interface. It is important to take account of dynamic defect interactions during irradiation involving migration, recombination, and annihilation. In addition, cascade shapes (i.e., instantaneous point defect distributions in collision cascades) strongly affect the efficiency of producing long-range migrating defects.[18] Previous studies have not investigated or discussed this effect.

Some papers on beam-assisted annealing or crystallization suggested that an ionization effect from the electronic energy

TABLE I. Irradiation conditions in this study.

Ion	Energy (MeV)	Average dose rate $(cm^{-2} s^{-1})$	Dose (cm^{-2})	Temperature (°C)
C	1.5–5.6	$2 \times 10^{12} - 5 \times 10^{12}$	$5.8 \times 10^{16} - 2.4 \times 10^{17}$	150–400
Si	1.5–5.6	$2 \times 10^{12} - 5 \times 10^{12}$	$3.8 \times 10^{16} - 9.0 \times 10^{16}$	250–400
Ge	1.5–5.6	$2 \times 10^{12} - 5 \times 10^{12}$	$3.4 \times 10^{15} - 1.1 \times 10^{16}$	250–400
Ag	1.5–5.6	$1 \times 10^{11} - 5 \times 10^{12}$	$2.3 \times 10^{15} - 7.0 \times 10^{15}$	250–400
Au	1.5–5.6	$2 \times 10^{10} - 5 \times 10^{12}$	$1.2 \times 10^{15} - 1.5 \times 10^{15}$	225–400

loss contributes to the defect annealing or crystallization.[19–22] Since defect ionization reduces migration energies of defects, activation energies of IBIEC can give important information on possible ionization effects. However, activation energies previously reported are widely different and range from 0.18 to 0.6 eV.[5,6,8,9,16,22–26] To date, the diversity of the measured activation energies has been considered to be due to experimental error or competing thermal epitaxy in many cases. No detailed study has been performed to establish the cause of this diversity.

In this study, the effects of ion mass on regrowth rates and activation energies have been investigated for five types of ion species from C to Au at energies of 1.5, 3.0, and 5.6 MeV. The use of different ion species makes it possible to change cascade density and dimensions and also adjust ratios between nuclear energy deposition and electronic energy deposition. In addition, MeV ion beams can produce almost uniform damage profiles and induce higher ionization than low-energy (below MeV) ion beams. This enables improved accuracy for measurement of regrowth rates and activation energies.

II. EXPERIMENTAL PROCEDURE

p-type (100)-oriented Si (B doped, 8–12 or 1–10 Ω cm) was first amorphized by Ge implantation at 200 keV to a dose of 1×10^{15} cm^{-2} at room temperature. The samples were cut into small pieces and then mounted on a temperature-controlled sample holder. Silver paste and metal clamps were used to fix the sample with good thermal contact. Before the irradiation for beam-induced crystallization, preannealing was performed at 450 °C for 1 h in vacuum to obtain sharp amorphous/crystalline interfaces. These processes resulted in an amorphous layer at the surface with a thickness of about 0.2 μm. Incoming beams were collimated by a 2-mm-diam graphite aperture or 3-mm-diam silicon aperture to define irradiated areas. The sample holder was tilted 7° off the ion beam direction to avoid channeling. The accuracy of irradiation doses was checked by Rutherford backscattering (RBS) of implanted Au ions. Five types of ion species (C, Si, Ge, Ag, Au) from tandem accelerators were used to stimulate IBIEC. Ion energies were 1.5, 3.0, and 5.6 MeV, with ion charge states of +1, +2, and +3, respectively. The irradiation conditions used in this study are summarized in Table I. A temperature rise of the irradiated area was estimated to be less than 1 °C on the assumption that the heat flow is one dimensional from the surface to the backside of the sample. The sample temperature was stabilized within ±2 °C during the irradiation as measured by thermocouples
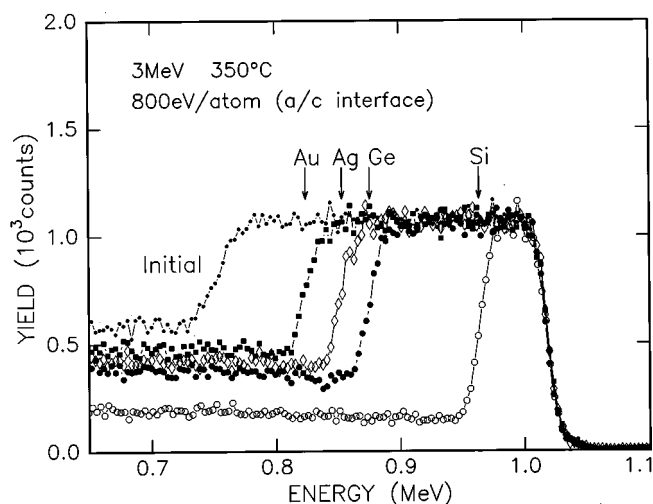
FIG. 1. Channeling spectra showing the difference in regrowth thicknesses among four different ion species (Au, Ag, Ge, and Si) at 3.0 MeV. Irradiation doses were adjusted to provide the same total nuclear energy deposition (800 eV/atom) to the initial amorphous/crystalline interfaces.

attached to the sample holder.

Regrowth thicknesses after irradiation were measured by ion-channeling analysis with 1.5 or 2 MeV He$^+$ beams from Van de Graaff accelerators. A glancing geometry with a scattering angle of 110° (for 1.5 MeV) or 100° (for 2 MeV) was used to enhance the depth resolution. Spot sizes for the channeling analysis were smaller than those for the crystal growth. Both the ion irradiation and channeling analyses were performed at two different laboratories with different implantation and analysis systems,[27] and both sets of results were consistent with each other. Distributions of nuclear energy deposition and vacancy concentrations were calculated by the TRIM code,[28] with a full cascade mode and an appropriate fitting procedure to avoid statistical fluctuations in calculated profiles. The displacement energy of Si was assumed to be 14 eV in the calculation.

III. RESULTS

Regrowth thicknesses were measured for different ion species to evaluate the contribution of nuclear energy deposition or defect generation. In order to reduce the experimental error for a light ion of which the regrowth thickness is much smaller than that of a heavy ion at the same dose, the irradiation dose was increased depending on the nuclear energy deposition. Figure 1 shows typical channeling spectra of the preannealed sample (initial) and samples after irradiation with 3.0 MeV Au, Ag, Ge, and Si at 350 °C. The dose rate was 2×10^{12} cm^{-2} s^{-1} for all ions. Different doses were chosen to provide the same total nuclear energy deposition at the depth of the initial amorphous/crystalline interface. The actual dose was increased from 1.5×10^{15} to 9.0×10^{16} cm^{-2} with decreasing ion mass. The regrowth thickness increased with decreasing ion mass, while the total nuclear energy deposition is nearly constant for all ions within the range of the measured depth. If the regrowth thickness is simply proportional to the nuclear energy deposition, it should be constant except for a small discrepancy due to the depth depen-
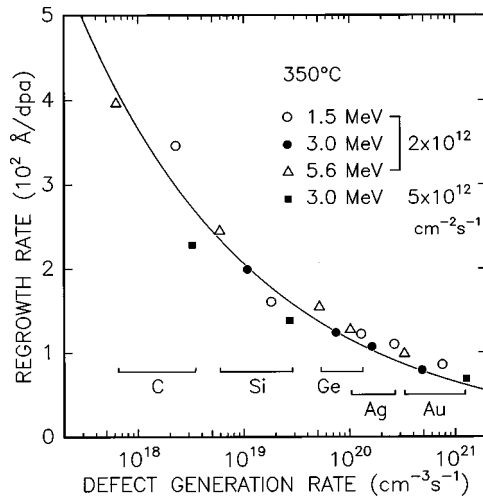
FIG. 2. Normalized regrowth rates as a function of defect generation rate for five ion species (C, Si, Ge, Ag, and Au) at three energies (1.5, 3.0, and 5.6 MeV) with two dose rates (2×10^{12} and $5 \times 10^{12} \, \mathrm{cm}^{-2} \, \mathrm{s}^{-1}$).

FIG. 3. Channeling spectra for 3.0 MeV Si and Ag. The $1 \times 10^{11} \, \mathrm{cm}^{-2} \, \mathrm{s}^{-1}$ Ag irradiation and $2 \times 10^{12} \, \mathrm{cm}^{-2} \, \mathrm{s}^{-1}$ Si irradiation provide the same nuclear deposition rate at the initial amorphous/crystalline interface. Irradiation doses were adjusted to provide the same total nuclear energy deposition (400 eV/atom) at the initial interface.

dence of the nuclear energy deposition (14% at maximum in this case). The observed differences between the regrowth thicknesses were much greater than the deviation in the nuclear energy deposition. Clearly, the crystallization process depends on the ion mass at constant average dose rate and for the same total nuclear energy deposition at the interface. This is ascribed to different average nuclear energy deposition rates of each ion species.

Figure 2 shows the regrowth rates normalized to displacements per atom (dpa) as a function of defect generation rate for five ion species (C–Au) at three energies (1.5–5.6 MeV) and two dose rates (2×10^{12} and $5 \times 10^{12} \, \mathrm{cm}^{-2} \, \mathrm{s}^{-1}$). The substrate temperature was 350 °C. The number of displacements per atom was calculated [from TRIM (Ref. 28)] from the number of displacements (vacancies) generated by ion or recoil collisions with substrate atoms at the interface without taking account of defect migration and annihilation. The number of displacements (vacancies) was calculated for both initial and final amorphous/crystalline interfaces, and the mean value was used for normalization. The normalized regrowth rate of C was approximately 4 times the normalized regrowth rate of Au for 1.5 and 5.6 MeV, noting that the defect generation rate of Au was approximately 3 orders of magnitude higher than that of C. This behavior is similar to the dose rate dependence previously reported for 300 keV ions.[16,17] Heera et al. proposed a diffusion-limited model for IBIEC and demonstrated the validity of their theoretical curve by fitting to previously published data on dose rate dependence.[29] The solid line in Fig. 2 is a least-squares fit of a theoretical curve based on this diffusion-limited model. A simplified functional form of the curve can be written as

$$r_\phi = c j^{-1/4}, \qquad (1)$$

where r_ϕ is the regrowth thickness normalized to the dose, c is a constant value, and j is the beam current. Under a simple approximation, Eq. (1) can be extended to

$$r_d = c' g^{-1/4}, \qquad (2)$$
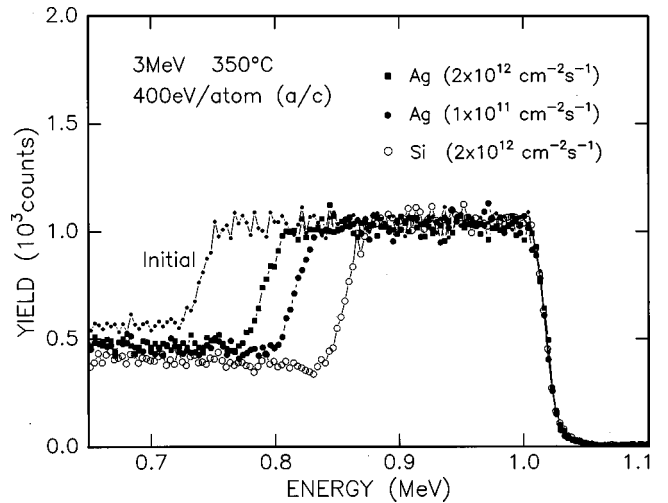
where r_d is the regrowth thickness normalized to the number of displacements, c' is a constant value, and g is the defect generation rate. Equation (2) is the case in Fig. 2. The curve is a good fit to the data points within experimental error for the irradiation conditions employed in Fig. 2.

Irradiation with different ion species at the same dose rate (beam current) changes the average nuclear energy deposition rate or defect generation rate quite dramatically. This substantially affects the crystal growth rate as observed, and this would appear to indicate that defect-defect interactions at high-energy deposition rates reduce the efficiency of crystal growth. In addition, the cascade size (local energy deposition density per ion) also varies dramatically with ion mass. Therefore, in order to identify the intrinsic nature of the mass effect, it is necessary to adjust the nuclear energy deposition rate or defect generation rate among different ion species. The channeling spectra in Fig. 3 show the result of such an experiment, where the dose rate of Ag was reduced to $1 \times 10^{11} \, \mathrm{cm}^{-2} \, \mathrm{s}^{-1}$ to provide the same average nuclear energy deposition rate at the interface as Si irradiation at a dose rate of $2 \times 10^{12} \, \mathrm{cm}^{-2} \, \mathrm{s}^{-1}$. The nuclear deposition rate of Ag is 20 times the nuclear deposition rate of Si with the same dose rate. The total doses were chosen for Ag ($2.3 \times 10^{15} \, \mathrm{cm}^{-2}$) and Si ($4.5 \times 10^{16} \, \mathrm{cm}^{-2}$) to obtain the same total nuclear energy deposition (400 eV/atom) at the initial interface. Figure 3 also shows the channeling spectrum for the Ag irradiation with the same dose rate ($2 \times 10^{12} \, \mathrm{cm}^{-2} \, \mathrm{s}^{-1}$) as the Si irradiation. When the dose rate is the same, the irradiation of the heavier Ag induced less regrowth than the irradiation of the lighter Si as shown in Fig. 2. However, even when the nuclear energy deposition rate was the same between Ag and Si, the Ag irradiation still induced less regrowth than the Si irradiation. The difference observed in Fig. 3 is ascribed to a cascade size effect separated from the average dose rate effect. In this case, the effect of increased cascade density and instantaneous energy
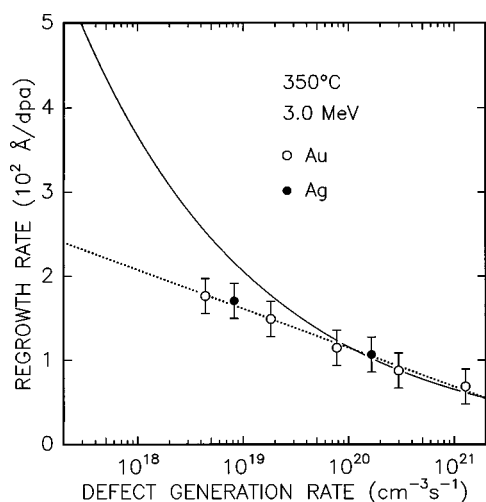
FIG. 4. Dose rate dependence of 3.0 MeV Au and Ag compared with the fitting curve for Fig. 2. The silver data were taken from the channeling spectra in Fig. 3. The solid line is the fitting curve shown in Fig. 2.

deposition density (instantaneous defect density) for the heavier ions probably reduced the efficiency of crystal growth.

Figure 4 directly compares the dose rate dependence of 3.0 MeV Au and Ag with the mass dependence shown in Fig. 2. Since the dose rate for Au ranged over 3 orders of magnitude, the implanted dose of Au was checked by RBS for each spot to calibrate the dose and dose rate. The influence of any leakage or current integration problems at low dose rates (i.e., low beam current) can be avoided by this calibration procedure. The solid line shows the fitting curve calculated for Fig. 2. The dose rate dependence of Au and Ag in Fig. 4 deviates from the fitting curve at low defect generation rates. The functional form for the dose rate dependence is different from the solid line and appears to fit a straight line (dotted line). The results in Fig. 4, taken together with those of Fig. 2, also indicate the role of the cascade size effect coexisting with the effect of the average defect generation rate.

Figure 5 shows an Arrhenius plot of regrowth rates normalized to the number of displacements as a function of reciprocal temperature for 3.0 MeV Si, Ge, and Au with a dose rate of $2 \times 10^{12} \, \text{cm}^{-2} \, \text{s}^{-1}$. Regrowth thicknesses were calculated as differences between irradiated and unirradiated (control) samples. The control samples underwent the same temperature treatments as the irradiated samples, and hence pure thermal epitaxy can be neglected in this case. Different doses were used for each ion in the range from 1.5×10^{15} to $4.5 \times 10^{16} \, \text{cm}^{-2}$ to obtain appropriate regrowth thicknesses and reduce experimental error. The regrowth thickness measured by the channeling measurement was normalized to the number of displacements in the same way as Fig. 2. Activation energies determined from Fig. 5 were 0.29 ± 0.02, 0.29 ± 0.01, and $0.38 \pm 0.02 \, \text{eV}$ for Si, Ge, and Au, respectively. The error values of each activation energy are the standard deviations determined from the least-squares fitting calculation. Figure 6 also shows a similar Arrhenius plot of the regrowth rates normalized to the number of displacements for 3.0 MeV C, Si, and Au with a dose rate of $5 \times 10^{12} \, \text{cm}^{-2} \, \text{s}^{-1}$. The doses used were in the range from
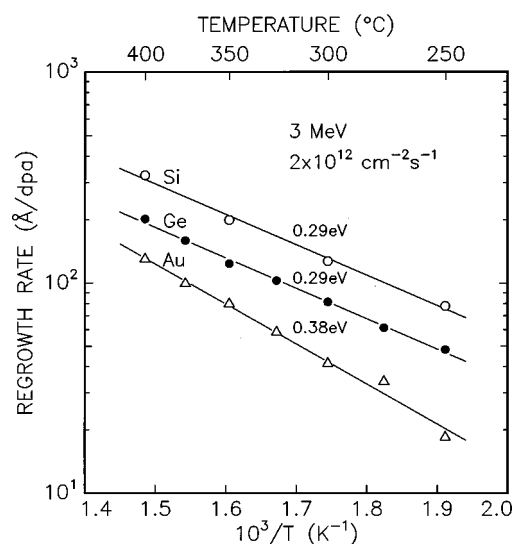
FIG. 5. Temperature dependence of regrowth rates normalized to the number of displacements for 3.0 MeV Si, Ge, and Au with a dose rate of $2 \times 10^{12} \, \text{cm}^{-2} \, \text{s}^{-1}$.

1.2×10^{15} to $2.4 \times 10^{17} \, \text{cm}^{-2}$ in this case. The regrowth thickness for Au at 225 °C was measured to be almost zero (not shown in Fig. 6), and this is therefore close to the zero growth temperature between crystallization and interfacial amorphization regimes. We note that the zero growth temperatures for other irradiations in Figs. 5 and 6 should be less than 225 °C because of the relationship between zero growth temperature, dose rate, and ion mass.[11] From Fig. 6, activation energies for Si and Au were 0.27 ± 0.01 and $0.40 \pm 0.02 \, \text{eV}$, respectively, which are essentially the same as those obtained for the lower dose rate in Fig. 5. The activation energy of C appeared to be temperature dependent. The temperature regime for C can be conveniently divided into 2 and activation energies were calculated as $0.18 \pm 0.02 \, \text{eV}$ (150–275 °C) and $0.37 \pm 0.01 \, \text{eV}$ (275–400 °C).

Some activation energies published to date have been determined from regrowth rates normalized to dose.[6,23,24] Since
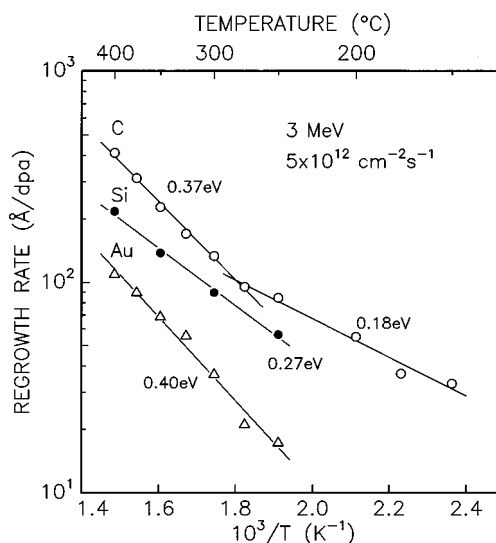
FIG. 6. Temperature dependence of regrowth rates normalized to the number of displacements for 3.0 MeV C, Si, and Au with a dose rate of $5 \times 10^{12} \, \text{cm}^{-2} \, \text{s}^{-1}$.

the regrowth rates normalized to the number of displacements can suffer from errors caused by the displacement calculation, we also determined activation energies from the regrowth rates normalized to dose. Results obtained were in good agreement with the activation energies determined from Fig. 6. Therefore, the difference between the two methods was negligible in this study.

IV. DISCUSSION

Solid-phase epitaxy of Si is strongly influenced by the presence of various impurities in amorphous layers.[30] This study aims to investigate the ion mass effects caused by the difference in radiation damaging effects, whereas the impurity effect is a chemical or electronic effect and different from a radiation damage effect. Therefore, it is necessary to first discuss and eliminate any influence of the impurity effect of irradiated ions themselves. Generally speaking, the projected ranges of irradiated ions in this study were always deeper than the amorphous/crystalline interface and almost all the implanted ions are distributed far from the amorphous layer. A heavy ion has a shallower projected range than a light ion, but the dose for the heavy ion was always lower than that of the light ion to obtain a similar regrowth thickness. Hence an impurity concentration in the amorphous layer does not increase very much even in the case of a heavy ion with a shallower projected range. Indeed, there is no impurity effect of implanted Si on the crystalline growth and the influence of Ag is expected to be negligible.[31] The concentration of C, Ge, or Au at the amorphous/crystalline interface was estimated to be less than 0.1 at. %. At this concentration, the impurity effects on solid-phase epitaxy are negligible.[30,31] Note that all samples have a Ge distribution from the amorphizing implant, with a peak concentration of about 0.2 at. %. Despite this, the growth rate through this layer was nearly constant for ions of constant nuclear energy deposition and did not vary with changing Ge concentration. In any case, Priolo et al. measured activation energies of the IBIEC process for Si doped with B, P, and Ge.[9] They concluded that the activation energy was independent of the dopant within experimental accuracy. Based on these considerations, we conclude that the results obtained in this study are caused by differences in the radiation-damaging effects of ion species (i.e., ion mass effects) and not the implanted ion itself.

A clear average dose rate dependence for MeV ions is observed as shown in Fig. 4. This result itself is illuminating with regard to the operative mechanism of IBIEC. There have been some previous dose rate data mainly for medium or low energies below 1 MeV.[16,17,32] Because of possible problems with beam-heating effects and only a weak dose rate dependence, there have previously been no systematic data for MeV ions except for the data near the zero growth temperature.[11] The current study substantially improved the accuracy of such measurements over larger temperature and dose rate ranges. Small spot sizes and low average dose rates were used to minimize beam heating effects. The use of Au ions allowed us to calibrate dose and dose rate by measuring the RBS of implanted Au atoms in the sample.

A significant average dose rate dependence of IBIEC growth rate (Fig. 4) implies that the defects responsible for
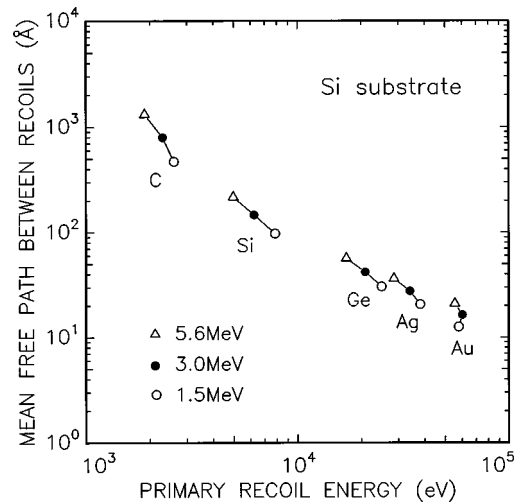
FIG. 7. Primary recoil energy and mean free path between primary collision events in Si for ions used in this study. The weighted-average recoil energy given by Averback et al. was used for this plot (Ref. 34). The mean free path was defined as a mean distance between collision events in which projectile ions provide target atoms with energies more than a displacement energy (Ref. 33).

IBIEC survive long after the initial annihilation process within individual cascades. Linnros and Holmen measured a frequency dependence of regrowth rates of IBIEC with pulsed ion beams, where the time constant of the process was determined to be of the order of 0.3 s.[16] This value is many orders of magnitude longer than the time scale for defect interactions within a collision cascade (of the order of a picosecond) as calculated by molecular dynamics simulations.[33] Our dose rate results support this conclusion, but also suggest that defect interactions, which are enhanced when dose rates (defect production rates) are higher, lower the efficiency of IBIEC.

The comparison of the dependences of IBIEC on ion mass and dose rate as embodied in Figs. 2 and 4 raises some interesting issues relating to defect interactions and their effects on IBIEC. In the dose rate experiments (Fig. 4), the same ion was used at different dose rates and hence sizes and densities of collision cascades are statistically identical for all (similar ion) data points. On the other hand, different ions are used at the same average dose rates in the case of the mass dependence experiments (Fig. 2). For example, Fig. 7 quantifies this difference for ion species used in this study, where the mean free path between collisions, which produce primary recoil atoms, is plotted as a function of the averaged primary recoil energy. Mean-free-path calculations used the method described in Ref. 33, and the average primary recoil energy was found as described in Ref. 34. For the irradiation energies used in this work, Au has a 2 orders of magnitude smaller mean free path for recoiling collisions than C. In addition, the average recoil energies are more than 20 times higher for Au than C. Since the number of point defects generated roughly scales with average recoil energy, the overall cascade for heavy ions such as Au consists of overlapping subcascades involving a very high density of point defects. On the other hand, light ions give rise to smaller, well-separated subcascades and the overall cascade has quite dilute point defect distributions. We also note that changing

the ion mass is more significant than changing the ion energy in terms of the density of point defect distributions in this study. It is additionally important to note that, at the temperatures used in this study, point defects generated in cascades start to diffuse after cascade quenching and some of them recombine to annihilate or form more complex defects. Hence the nature of residual defects should strongly depend on defect interactions and on the size and density of cascades.

The issues discussed above, in terms of ion mass and cascade density effects on the formation of stable defects, have been previously extensively developed for defect formation in metals.[34,35] For example, a projectile-mass dependence of the amorphization of metals or metallic alloys such as Cu, $NiAl_3$, CuTi, and Zr_3Al was observed and interpreted in terms of differences in the point defect density within individual cascades.[35–38] In semiconductors and Si in particular,[39,40] ion mass and cascade effects on amorphization have also been studied. Similar trends on irradiated metals were obtained for Si amorphization at low temperatures under electron and ion beam irradiation.[41] Although there has been no previous study on the effect of cascade size and density on migrating defects and induced crystallization in silicon, there are some reports on both metals and semiconductors of relevance for the present study. For example, Rehn *et al.* measured the relative efficiency of different ions (H, He, Li, Ni, Kr at MeV energies) for producing freely migrating defects by radiation-induced segregation of Ni-Si alloy.[18] They observed a strong mass dependence of relative efficiency for producing long-range migrating defects, where the efficiency decreased from 48% to <2% with increasing ion mass. Indeed, Keskitalo and co-workers reported an ion mass dependence of defect structures (ratio of the divacancy V_2 and the vacancy-oxygen complex VO) measured by deep-level transient spectroscopy (DLTS) for MeV ions (H, He, O, S) implanted into Si.[42] They ascribed the change in VO/V_2 ratio to different cascade size (or density) depending on the ion mass.[42,43] Therefore, it is important to take into account the instantaneous defect generation rate (instantaneous nuclear energy deposition rate), namely, the local density of point defects within individual cascades just after cascade formation, in addition to the average defect generation rate (average nuclear energy deposition rate). Both effects are clearly important.

Based on the above arguments, we attribute the difference between the energy deposition rate for different masses (mass dependence in Fig. 2) and the dose rate dependence for the same mass (Fig. 4) to cascade density effects. Such effects involve large changes in the instantaneous defect generation rate per ion for different mass ions (see Fig. 7) even when the average energy deposition rate is constant. In the paper on the diffusion-limited model for IBIEC,[29] Heera *et al.* demonstrated a fit of a $j^{-1/4}$ curve [see Eq. (1)] to dose rate data, which is actually a fit of an $Sn^{-1/4}$ curve (Sn: average nuclear energy deposition) when different ion masses are involved.[44] Essentially, the $j^{-1/4}$ curve, according to Heera *et al.*, should include both effects of the average defect generation rate (dose rate dependence) and instantaneous defect generation rate (mass dependence). However, the dose rate dependence data in Fig. 4 deviate from the mass dependence curve ($\propto j^{-1/4}$) at lower defect generation
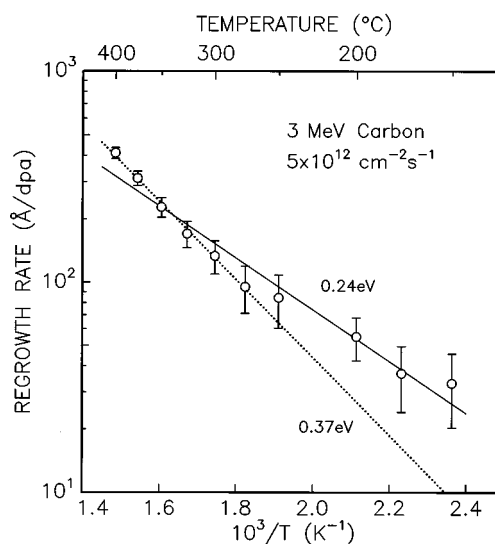
FIG. 8. A single least-squares fit (solid line) to all the carbon data of Fig. 6. The activation energy from the slope of the solid line was 0.24 eV. For comparison, another least-squares fit to the 275–400 °C regime is shown (dotted line).

rates. This implies that the assumption used in the diffusion-limited model does not adequately cater to the difference between these two effects. Their paper showed that the formula, derived from the diffusion-limited model, is a good fit to the regrowth rates previously published. However, the results in the present study show that their formula does not fit extended dose rate data for the same ion. Our results, therefore, indicate that the concentration of ''defects,'' which survive recombination and annihilation following collision cascade quenching and which mediate IBIEC, can be significantly influenced by both cascade density and average energy deposition rates.

Previous studies on IBIEC argued for a single activation energy which represents the rate-limiting step of IBIEC, but in practice the measured activation energies were different and ranged from 0.18 to 0.6 eV.[5,6,8,9,16,22–26] The differences among reported values were considered to be due to experimental error, competing thermal epitaxy in higher temperature regimes, and beam-induced amorphization at lower temperatures. However, the data in Figs. 5 and 6 also showed several activation energies from 0.18 to 0.40 eV, where differences are larger than error values calculated from the least-squares fitting and where extreme care was taken to minimize low- and high-temperature effects. Thus our results unequivocally indicate that IBIEC cannot be characterized by a single activation energy. To some extent, our measured activation energies are consistent with those previously reported values. In general, when a heavy ion or a lower energy ion is used, higher activation energies are obtained, and when light ion with a higher energy is used, lower activation energies are obtained. Interestingly, a least-squares fit of a single line for all the C data (150–400 °C), as shown in Fig. 8 (solid line), exhibits an apparent activation energy of 0.24 eV, which is lower than the activation energies of Si, Ge, and Au. Hence our data indicate that the activation energy increases as the ion mass and the instantaneous energy deposition density is increased. It should be noted for Fig. 8 that another fit (dotted line) to the higher temperature regime

(275–400 °C) deviates at the lower temperatures more than the length of error bars and hence it is appropriate to have two fits to the different temperature regimes as shown in Fig. 6. In the case of activation energy, there appears to be a negligible dose rate effect (for similar ions).

First, we discuss the possible cause of this activation energy difference in terms of electronic energy deposition (Se) or ionization. Based on the reported activation energies of about 0.3 eV, it has been proposed that the rate-limiting defect responsible for IBIEC may be a neutral vacancy V^0 of which the migration energy is 0.33 eV.[5] An ionized vacancy V^{2-} has a lower migration energy (0.18 eV) than the neutral vacancy, and if ionization increases the mobility of such defects, then it may enhance the crystallization.[2,23] If defect ionization is effective in IBIEC, a reduction of the activation energy can be expected with increasing ionization/defect generation ratio (i.e., Se/Sn). In this study, four types of ion species C, Si, Ge, and Au at 3 MeV were used for the activation energy measurements. The ionization energy loss (Se) at the depth of 0.2 μm is estimated to be $1-3 \times 10^2$ eV/Å/ion, nearly the same for the four ion species. The ionization energy per displacement (vacancy) at 0.2 μm is 2×10^4, 4×10^3, 3×10^2, and 1×10^2 eV/vacancy for C, Si, Ge, and Au, respectively. These values are different by more than two orders of magnitude between C and Au. Although at first sight there may be a trend for the lowest ionization/vacancy value (Au) to have the highest activation energy of about 0.4 eV, a close examination of the data does not indicate consistency. For example, Ge and Au are close in terms of ionization/vacancy values, but have a large activation energy difference. On the other hand, there is no difference between the Si and Ge values within experimental error. Thus no consistent relationship was found between the activation energy and possible ionization effects, and we believe that ionization is a minor contributing factor to IBIEC.

Jackson proposed a theoretical model which apparently fits well to selected experimental data such as the dose rate data near the zero growth temperature and a pulsed-beam frequency dependence.[45] He mentioned that the slope of the flat portion of the temperature dependence curve (the region where we extract the low IBIEC activation energies between thermal and amorphization regimes) has no physical significance and should not be attributed to a separate activation process. If the Jackson model is correct, it is natural to observe various apparent activation energies depending on ion mass and dose rate. To check whether our IBIEC data are consistent with the Jackson model, we can examine the functional form obtained by Jackson for the temperature regime where IBIEC dominates and compare it with the form of our data. In this regime, Jackson assumed that the rate at which beam-induced defects annihilated at or close to the interface was fast compared with the ion arrival rate. Based on a single defect process controlling layer-by-layer crystallization and amorphization at the interface, he derived the following relation for the crystal growth rate (growth thickness normalized to dose) r_ϕ:

$$r_\phi = c_1(c_2 - E/kT),\qquad(3)$$

where E is the activation energy for the defect migration, T is the irradiation temperature, and c_1 and c_2 are constants as-
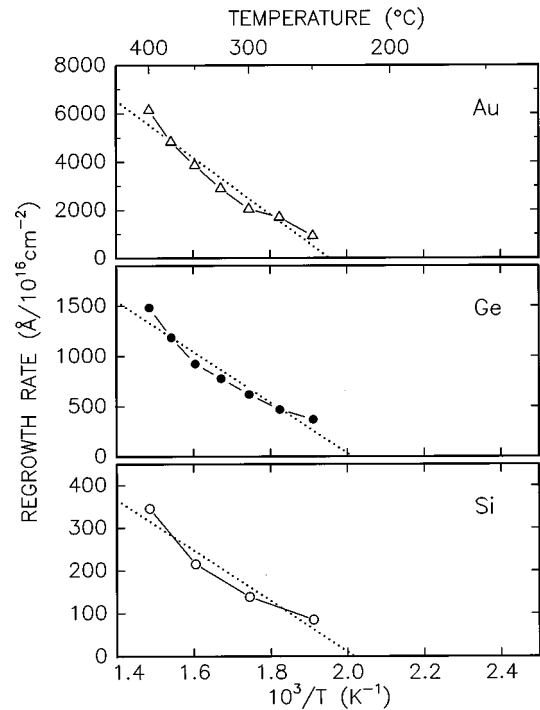
FIG. 9. Linear regrowth rate normalized to dose as a function of reciprocal temperature for 3 MeV Au, Ge, and Si ions with a dose rate of 2×10^{12} cm^{-2} s^{-1} (same as Fig. 5). The dotted lines are least-squares fits to data points.

sociated with damage production and annihilation. In the case of Eq. (3), Jackson actually assumed that the ratio of the defect decay rate to the ion arrival rate (which he called γ) was large ($\gamma \gg 1$). In the Appendix, we give further details of the functional forms of the rate of interface motion according to the Jackson model and their relation to the present study. What is important here is that r_ϕ is linearly dependent on $1/T$ at constant dose rate, according to Eq. (3). Indeed, Jackson applied Eq. (3) to selected data from Ref. 46 with some success in the temperature range close to the zero growth temperature.

Figures 9 and 10 examine the validity of Eq. (3) for our data from Figs. 5 and 6. The vertical axes of Figs. 9 and 10 are not logarithmic scales, but linear, different from the Arrhenius plots in Figs. 5 and 6, and represent growth rates normalized to a dose of 1×10^{16} cm^{-2} at a constant dose rate. If Eq. (3) is valid, the data points should fit to a linear function. The dotted lines drawn in Figs. 8 and 9 represent least-squares fits of a straight line to the data points. A similar nonlinear behavior is observed for all ion species and is particularly significant for C, where measured growth rates are substantially higher than the fitting lines at low and high temperatures. Based on the consistency of the data for all masses, it is difficult to see how experimental error or other factors could have caused this discrepancy from a linear form for the following reasons. We note again that growth thicknesses were calculated with controls which underwent the same temperature treatment as ion-irradiated areas, and hence the contribution of pure thermal epitaxy can be neglected. Thus the higher regrowth rates in the high-temperature regime of Figs. 9 and 10 are not due to a contribution from thermal epitaxy. We can also explore the lower-temperature regime of Figs. 8 and 9. In this case, we
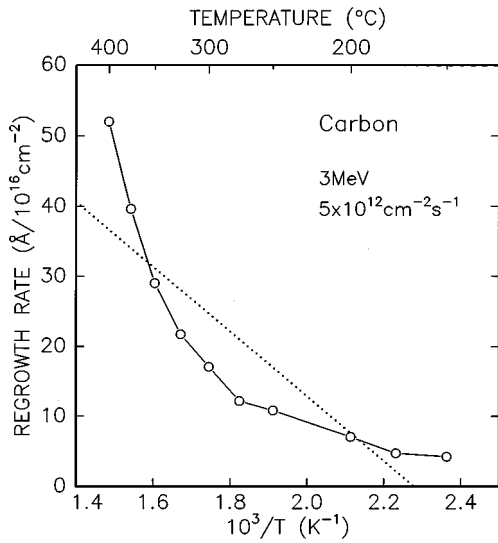
FIG. 10. Linear regrowth rate normalized to dose as a function of reciprocal temperature for 3 MeV C ions with a dose rate of $5 \times 10^{12}\,\mathrm{cm}^{-2}\,\mathrm{s}^{-1}$ (same as Fig. 6). The dotted line is a least-squares fit.

can examine the validity of the assumption, in deriving Eq. (3), that γ is large ($\gamma \gg 1$). As we show in the Appendix, when $\gamma < 1$, Jackson finds that the growth rate is given by

$$r_\phi = c_3 \exp(-E/2kT), \qquad (4)$$

where c_3 is another constant depending on the irradiation conditions. When γ is close to 1, the functional form of r_ϕ changes from Eq. (4) (at the low-temperature regime) to Eq. (3) (at the high-temperature regime) with increasing temperature, showing an overall nonlinear behavior. However, we note again that Jackson fitted Eq. (3) ($\gamma \gg 1$) to Xe growth data on both sides of the zero growth temperature. In the case of Figs. 8 and 9, we are at temperatures considerably greater than the zero growth temperature and hence we expect that γ should be >1 [i.e., Eq. (3) is valid]. The question may be asked as to whether γ remains >1 for the low-temperature C data of Fig. 10, since, for the dilute C cascades, defects may take much longer times to annihilate at lower temperatures. Nevertheless, a linear relationship does not fit the C data very well even above 300 °C. Therefore, based on the above arguments, our data are not consistent with the functional form of interface growth based on the Jackson model. In fact, there are other discrepancies noted in the literature at low temperatures.[29,47] For example, Goldberg recently reported that several activation energies are observed for the zero growth temperature as a function of dose rate,[47] and yet the Jackson model assumes a single activation energy (1.2 eV) for zero growth. These results, taken together, strongly suggest that the Jackson model is oversimplistic for treating IBIEC and IBIIA in terms of a single (simple) defect controlling both crystallization and amorphization processes.

Carter and Nobes have proposed an alternate approach to crystallization and amorphization induced by ion irradiation,[48] which has some attraction based on the results of our study. They basically considered the motion of an amorphous/crystalline interface under ion irradiation to be controlled by three activated processes, each of which was

dominant in a particular temperature regime. The key difference between this model and that of Jackson is that Carter and Nobes generally assumed that up to three rate-limiting (defect-mediated) processes may describe interface motion, according to the formula

$$R = R_a - R_t - R_i, \qquad (5)$$

where R is the rate of interface motion, R_a is an amorphization term, R_t is the normal thermal epitaxy term, and R_i is an ion-induced epitaxy term. R_a includes both the generation of an amorphous zone during ion bombardment, which depends on the nuclear energy deposition rate, and a temperature-dependent (exponential) shrinkage term, which allows for annealing of this amorphous region through defect interaction following cascade quenching. R_t and R_i are exponentially temperature dependent as expected and given by

$$R_t = c_t \exp(-E_t/kT) \qquad (6)$$

and

$$R_i = c_i \exp(-E_i/kT), \qquad (7)$$

where c_t and c_i are constant values and E_t and E_i are the activation energies for thermal [2.7 eV (Ref. 7)] and ion-induced epitaxy, respectively. Three temperature regimes were identified where (i) thermal epitaxy (R_t) dominates crystallization at high temperatures ($>400\,°C$), and (ii) the amorphization term (R_a) dominates at low temperatures where the R_t and R_i terms are negligible. R_a is both mass dependent and dose rate dependent since the rate of growth of amorphous zones depends on the rate of damage production and defect annihilation. Finally, (iii) at intermediate temperatures, IBIEC dominates. It may be possible that two of the terms in Eq. (5) are significant over a limited temperature range. For heavy ions, for example, both R_a and R_i could be operative over a reasonably wide temperature window. This would effectively increase measured activation energies for IBIEC, if this lower-temperature range was included in the measurement of IBIEC activation energies. However, even if we exclude the lowest two or three temperature values for Au from Figs. 5 and 6, the activation energy for Au would not be substantially lowered. This is also true for the Ge and Si data. Our result for C irradiation is also clearly not consistent with an assumption of a single activation energy. Although most of the temperatures examined for C are well separated from the thermal epitaxy regime at high temperature and the amorphization regime at low temperature, we appear to measure more than one activation energy for C. Thus our data would appear to suggest more than one activation energy for IBIEC, covering the ion mass, dose rates and temperatures investigated, whereas Carter and Nobes argue for a single activation energy. In keeping with the simplicity of this model, however, it is tempting to add more than one activation term in the IBIEC regime, corresponding to different rate-limiting processes. Finally, in view of our dose rate data in Fig. 4, the Carter-Nobes model predicts that R_i should be proportional to dose rate for the same ion mass, as we observed.

The origin of the several activation energies can thus be ascribed to several competing defect-limiting processes responsible for IBIEC, involving more than one type of defect.

Indeed, ion irradiation, depending on ion mass, can produce a range of metastable, simple, and more complex defects which can dissociate, annihilate, and interact with the amorphous/crystalline interface. Concentrations of each type of defect will depend on many factors such as cascade shapes, diffusivities, interaction cross sections, and dissociation energies. The irradiation of heavy ions generates dense cascades which enhance defect annihilation or interactions to produce more complex defect structures. On the contrary, the irradiation with light ions generates dilute cascades which decrease annihilation and increase the time constant for defect interactions. Hence the balance of various defect types would depend on both average and instantaneous defect generation rates determined by ion mass. The dissociation, migration, interaction, and evolution of defects are clearly temperature dependent. Consequently, irradiation with different ion species at different temperature would be expected to result in different activation energies for IBIEC if it is mediated by several competing defect-interaction processes. In this regard, it is interesting to note that a similar conclusion has been made to explain observations in the lower-temperature range where defect production and amorphization dominate (i.e., IBIIA regime). For example, Goldberg *et al.* reported on activation energies of end-of-range amorphization of Si irradiated with different ion species (from C to Xe) and noted that apparent activation energies for the process varied from 0.7 to 1.7 eV depending on ion mass.[49] Their result suggested that contributions of several defect interactions caused a large variation in the measured activation energy which characterized the amorphization process for different ion mass.

Having concluded that several defect-limiting processes appear to control IBIEC, it is reasonable to ask which defect types are most likely to be involved and how far from the interface can they be generated. Treating the second of these two issues first, we note that our present data do not add up to what is already known. Indeed, we have assumed, based on previous studies showing the IBIEC rate to scale with the nuclear energy deposition rate at the interface, that defect generation at or very close to the interface is dominant. Previous studies have given no strong evidence for a role of defects migrating more than ten monolayers from the interface.[5] In terms of which defects may be contributing, there have been several suggestions. Earlier we indicated the attraction of vacancies of various charge states as a result of the similar values of migration energies of these defects compared with IBIEC activation energies. However, the correlation between the two processes is not close enough, particularly with the wide IBIEC activation energies measured in this study, to suggest that vacancy migration is the rate-limiting process controlling IBIEC. Ultimately, it is a bond-breaking event at the interface which completes crystallization and early IBIEC studies suggested that the rate-limiting process of IBIEC is related to the migration energy of dangling bonds (or kinks) along the interface.[45,50] This simple model is also questionable in view of the several activation energies measured in this study. On the other hand, the rate-limiting effect may be the availability of appropriate crystallization sites at the interface, which are controlled by the dissociation of more complex defects at or near the interface.

Finally, it is known that divacancies in Si are annealed out at a temperature of 200–300 °C.[51,52] This temperature is very close to the transition regime where the C activation energy in this study appears to change from a low to a high value (Fig. 6). Linnros and co-workers attributed divacancy dissociation to the origin of the time constant in IBIEC and the reversal interface motion at low temperatures.[16,46] Thus the result of C may support divacancy dissociation as one of the defect processes responsible for IBIEC in a limited temperature regime. However, the operative mechanism of IBIEC over wide temperature and energy deposition regimes is clearly more complex than previous single-defect models suggest. Based on our observations, it is more natural to assume that several competing defect interactions and dissociation of defect complexes (defect soup) provide the crystallization sites at the interface that mediate IBIEC.

V. CONCLUSION

This study examined the effects of ion mass on regrowth rates and activation energies in ion-beam-induced epitaxial crystallization of Si with five types of ions at MeV energies. A strong mass dependence was observed for both the regrowth rate and activation energy. The mass dependence did not simply translate to an average dose rate dependence. This implies that the instantaneous defect generation rate determined by cascade shapes and defect density is an important factor controlling IBIEC in addition to average defect generation rates. Several activation energies (0.18–0.40 eV) were observed depending on ion mass and temperature, indicating that IBIEC cannot be characterized by a single activation energy. There was no consistent relationship between ionization and measured activation energies under the conditions of this study. The results of this study are therefore inconsistent with previously proposed models assuming that a discrete defect controls IBIEC. More complex processes involving several types of defect interaction may be operative in IBIEC.

APPENDIX

Jackson defined the parameter γ as the ratio of the defect decay rate to the ion arrival rate [Eq. (10) in the Jackson paper]:

$$\gamma = N_0 \sigma^2 a \tau_0 / \tau_j \qquad (A1)$$

$$= N_0 \sigma^2 a \tau_0 \nu_0 \exp(-E/kT), \qquad (A2)$$

where N_0 is the defect density created at the interface inside the defect cylinder along the ion track, σ^2 is the capture cross section for one defect by another, a is the lattice pa-

rameter, τ_0 is the period of ion arrivals, and τ_j is the time between defect jumps which can be described by an Arrhenius-type function with a preexponential factor ν_0 and an activation energy E (k is the Boltzmann constant and T the temperature). A crystal growth rate can be written [Eq. (18) in the Jackson paper] as

$$R = (\Lambda l_0^2 \phi / \sigma^2) \ln\{1 + (\gamma/2)[1 + (1 + 4/\gamma)^{1/2}]\} - V_\alpha \phi, \tag{A3}$$

where Λ is the crystal volume created per defect jump, l_0^2 is the diameter of defect distributions along the ion path, ϕ is the incident ion flux, and V_α is the volume of amorphous zone created by each ion. For large γ ($\gamma \gg 1$), Jackson derived a formula for a crystal growth rate normalized to the dose [Eq. (21) in the Jackson paper] as

$$R/\phi = (\Lambda l_0^2 / \sigma^2)[\ln(\phi_0/\phi) - E/kT], \tag{A4}$$

where we assume that the amorphization term $V_\alpha \phi$ is negligible. If we define constants $c_1 = (\Lambda l_0^2 / \sigma^2)$ and $c_2 = \ln(\phi_0/\phi)$, then Eq. (3) in the present paper is obtained since $r_\phi = R/\phi$:

$$r_\phi = c_1(c_2 - E/kT). \tag{A5}$$

For small γ ($\gamma \ll 1$), Eq. (A3) can be approximated by

$$R = (\Lambda l_0^2 \phi / \sigma^2) \gamma^{1/2}. \tag{A6}$$

From Eqs. (A2) and (A6), one can write, again assuming that the $V_\alpha \phi$ term is negligible

$$R = (\Lambda l_0^2 \phi / \sigma^2)(N_0 \sigma^2 a \tau_0 \nu_0)^{1/2} \exp(-E/2kT). \tag{A7}$$

If we define a constant $c_3 = (\Lambda l_0^2 / \sigma^2)(N_0 \sigma^2 a \tau_0 \nu_0)^{1/2}$, we obtain

$$R = c_3 \phi \exp(-E/2kT). \tag{A8}$$

The crystal growth rate normalized to the dose is

$$r_\phi = R/\phi \tag{A9}$$

$$= c_3 \exp(-E/2kT). \tag{A10}$$

This is Eq. (4) in the present paper.

---

*Present address: Osaka National Research Institute, AIST, 1-8-31 Midorigaoka, Ikeda, Osaka 563-8577, Japan.

[1] I. Golecki, G. E. Chapman, S. S. Lau, B. Y. Tsaur, and J. W. Mayer, Phys. Lett. **71A**, 267 (1979).

[2] J. Nakata and K. Kajiyama, Appl. Phys. Lett. **40**, 686 (1982).

[3] R. G. Elliman, J. S. Williams, W. L. Brown, A. Leiberich, D. M. Maher, and R. V. Knoell, Nucl. Instrum. Methods Phys. Res. B **19/20**, 435 (1987).

[4] F. Priolo and E. Rimini, Mater. Sci. Rep. **5**, 319 (1990).

[5] J. Linnros, B. Svensson, and G. Holmén, Phys. Rev. B **30**, 3629 (1984).

[6] J. S. Williams, R. G. Elliman, W. L. Brown, and T. E. Seidel, Phys. Rev. Lett. **55**, 1482 (1985).

[7] G. L. Olson, S. A. Kokorowski, J. A. Roth, and L. D. Hess, in *Laser-Solid Interactions and Transient Thermal Processing of Materials*, edited by J. Narayan, W. L. Brown, and R. A. Lemons, MRS Symposia Proceedings No. 13 (Materials Research Society, Pittsburgh, 1983), p. 141.

[8] A. La Ferla, S. Cannavò, G. Ferla, S. U. Campisano, E. Rimini, and M. Servidori, Nucl. Instrum. Methods Phys. Res. B **19/20**, 470 (1987).

[9] F. Priolo, A. La Ferla, and E. Rimini, J. Mater. Res. **3**, 1212 (1988).

[10] A. Leiberich, D. M. Maher, R. V. Knoell, and W. L. Brown, Nucl. Instrum. Methods Phys. Res. B **19/20**, 457 (1987).

[11] J. Linnros, R. G. Elliman, and W. L. Brown, J. Mater. Res. **3**, 1208 (1988).

[12] F. Priolo, C. Spinella, A. La Ferla, E. Rimini, and G. Ferla, Appl. Surf. Sci. **43**, 178 (1989).

[13] G. Lulli, P. G. Merli, and M. Vittori Antisari, Phys. Rev. B **36**, 8038 (1987).

[14] J. Linnros and G. Holmén, J. Appl. Phys. **59**, 1513 (1986).

[15] N. Kobayashi, M. Hasegawa, and N. Hayashi, Nucl. Instrum. Methods Phys. Res. B **80/81**, 790 (1993).

[16] J. Linnros and G. Holmén, J. Appl. Phys. **62**, 4737 (1987).

[17] V. Heera, R. Kögler, W. Skorupa, and R. Grötzschel, Nucl. Instrum. Methods Phys. Res. B **80/81**, 538 (1993).

[18] L. E. Rehn, P. R. Okamoto, and R. S. Averback, Phys. Rev. B **30**, 3073 (1984).

[19] J. Washburn, C. S. Murty, D. Sadana, P. Byrne, R. Gronsky, N. Cheung, and R. Kilaas, Nucl. Instrum. Methods Phys. Res. **209/210**, 345 (1983).

[20] M. Miyao, A. Polman, W. Sinke, F. W. Saris, and R. van Kemp, Appl. Phys. Lett. **48**, 1132 (1986).

[21] G. Lulli and P. G. Merli, Phys. Rev. B **47**, 14 023 (1993).

[22] J. Nakata, J. Appl. Phys. **79**, 682 (1996).

[23] J. Nakata, Phys. Rev. B **43**, 14 643 (1991).

[24] N. Kobayashi, H. Kobayashi, and Y. Kumashiro, Nucl. Instrum. Methods Phys. Res. B **40/41**, 550 (1989).

[25] B. Zeroual and G. Carter, Vacuum **42**, 525 (1991).

[26] J. M. Glasko, Master thesis, The University of Western Ontario, 1993.

[27] A. Kinomura, A. Chayahara, Y. Horino, Y. Mokuno, and K. Fujii, Nucl. Instrum. Methods Phys. Res. B **106**, 277 (1995).

[28] J. F. Ziegler, J. P. Biersack, and U. Littmark, *The Stopping and Range of Ions in Solids* (Pergamon, New York, 1986).

[29] V. Heera, T. Henkel, R. Kögler, and W. Skorupa, Phys. Rev. B **52**, 15 776 (1995).

[30] G. L. Olson and J. A. Roth, in *Handbook of Crystal Growth*, edited by D. T. J. Hurle (North-Holland, Amsterdam, 1994).

[31] D. C. Jacobson, R. G. Elliman, J. M. Gibson, G. L. Olson, J. M. Poate, and J. S. Williams, in *Beam-Solid Interactions and Transient Processes*, edited by M. O. Thompson, S. T. Picraux, and J. S. Williams, MRS Symposia Proceedings No. 74 (Materials Research Society, Pittsburgh, 1987), p. 327.

[32] J. S. Williams, W. L. Brown, R. G. Elliman, R. V. Knoell, D. M. Maher, and T. E. Seidel, in *Ion Beam Processes in Advanced Electronic Materials and Device Technology*, edited by B. R. Appleton, F. H. Eisen, and T. W. Sigmon, MRS Symposia Proceedings No. 45 (Materials Research Society, Pittsburgh, 1985), p. 79.

[33] See, for example, M. Nastasi, J. W. Mayer, and J. K. Hirvonen, *Ion-Solid Interactions: Fundamentals and Applications* (Cambridge University Press, Cambridge, England, 1996).

[34] R. S. Averback, R. Benedek, and K. L. Merkle, Phys. Rev. B **18**, 4156 (1978).

[35] R. S. Averback, J. Nucl. Mater. **108/109**, 33 (1982).

[36] M. Nastasi, J. M. Williams, E. A. Kenik, and J. W. Mayer, Nucl. Instrum. Methods Phys. Res. B **19/20**, 543 (1987).

[37] J. Koike, P. R. Okamoto, L. E. Rehn, and M. Meshii, J. Mater. Res. **4**, 1143 (1989).

[38] J. Koike, P. R. Okamoto, L. E. Rehn, and M. Meshii, Metall. Trans. A **21**, 1799 (1990).

[39] J. W. Corbett, J. P. Karins, and T. Y. Tan, Nucl. Instrum. Methods Phys. Res. **182/183**, 457 (1981).

[40] R. S. Averback and D. N. Seidman, Mater. Sci. Forum **15−18**, 963 (1987).

[41] D. N. Seidman, R. S. Averback, P. R. Okamoto, and A. C. Baily, in *Electron Microscopy of Materials*, edited by W. Krakow, D. A. Smith, and L. W. Hobbs, MRS Symposia Proceedings No. 31 (Materials Research Society, Pittsburgh, 1986), p. 349.

[42] N. Keskitalo, A. Hallén, L. Josyula, and B. G. Svensson, Nucl. Instrum. Methods Phys. Res. B **127/128**, 410 (1997).

[43] A. Hallén and B. G. Svensson, Nucl. Instrum. Methods Phys. Res. B **80/81**, 106 (1993).

[44] Irradiation of different ion species with different Sn values changes nuclear energy deposition rates. When a dose rate is constant, the nuclear energy deposition rate is proportional to Sn. Hence the $Sn^{-1/4}$ curve in Fig. 2 has the same meaning as the $j^{-1/4}$ curve.

[45] K. A. Jackson, J. Mater. Res. **3**, 1218 (1988).

[46] W. L. Brown, R. G. Elliman, R. V. Knoell, A. Leiberich, J. Linnros, D. M. Maher, and J. S. Williams, in *Microscopy of Semiconducting Materials*, edited by A. G. Cullis, IOP Conf. Proc. No. 87 (Institute of Physics, Bristol, 1987), p. 61.

[47] R. D. Goldberg, Ph.D. thesis, The University of Melbourne, 1996.

[48] G. Carter and M. J. Nobes, J. Mater. Res. **6**, 2103 (1991).

[49] R. D. Goldberg, J. S. Williams, and R. G. Elliman, Nucl. Instrum. Methods Phys. Res. B **106**, 242 (1995).

[50] F. Priolo, C. Spinella, and E. Rimini, Phys. Rev. B **41**, 5235 (1990).

[51] G. D. Watkins and J. W. Corbett, Phys. Rev. **138**, A543 (1965).

[52] F. L. Vook and H. J. Stein, Radiat. Eff. **2**, 23 (1969).